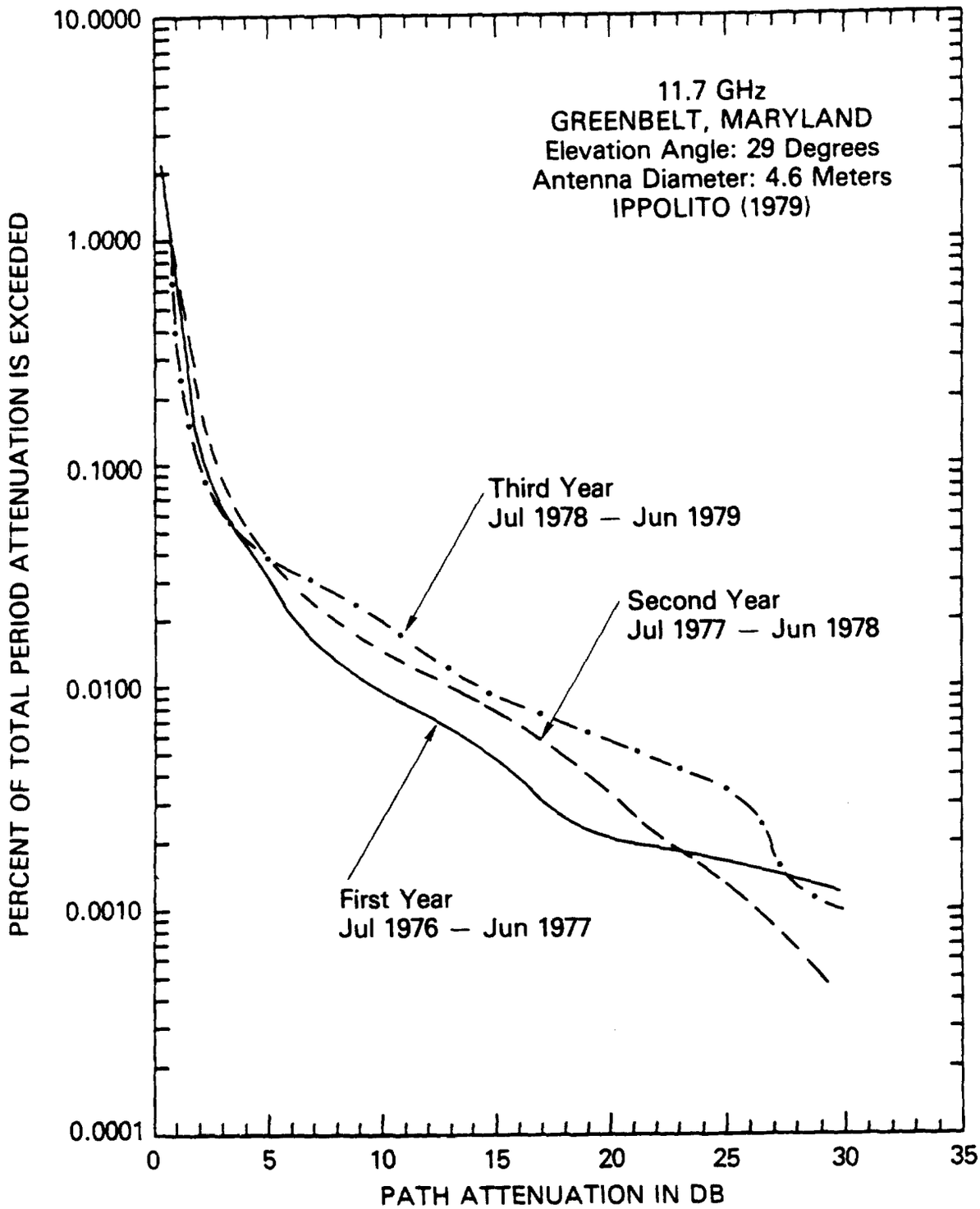

Figure 5.4-3. Annual 11.7 GHz Attenuation Distributions for Greenbelt, MD

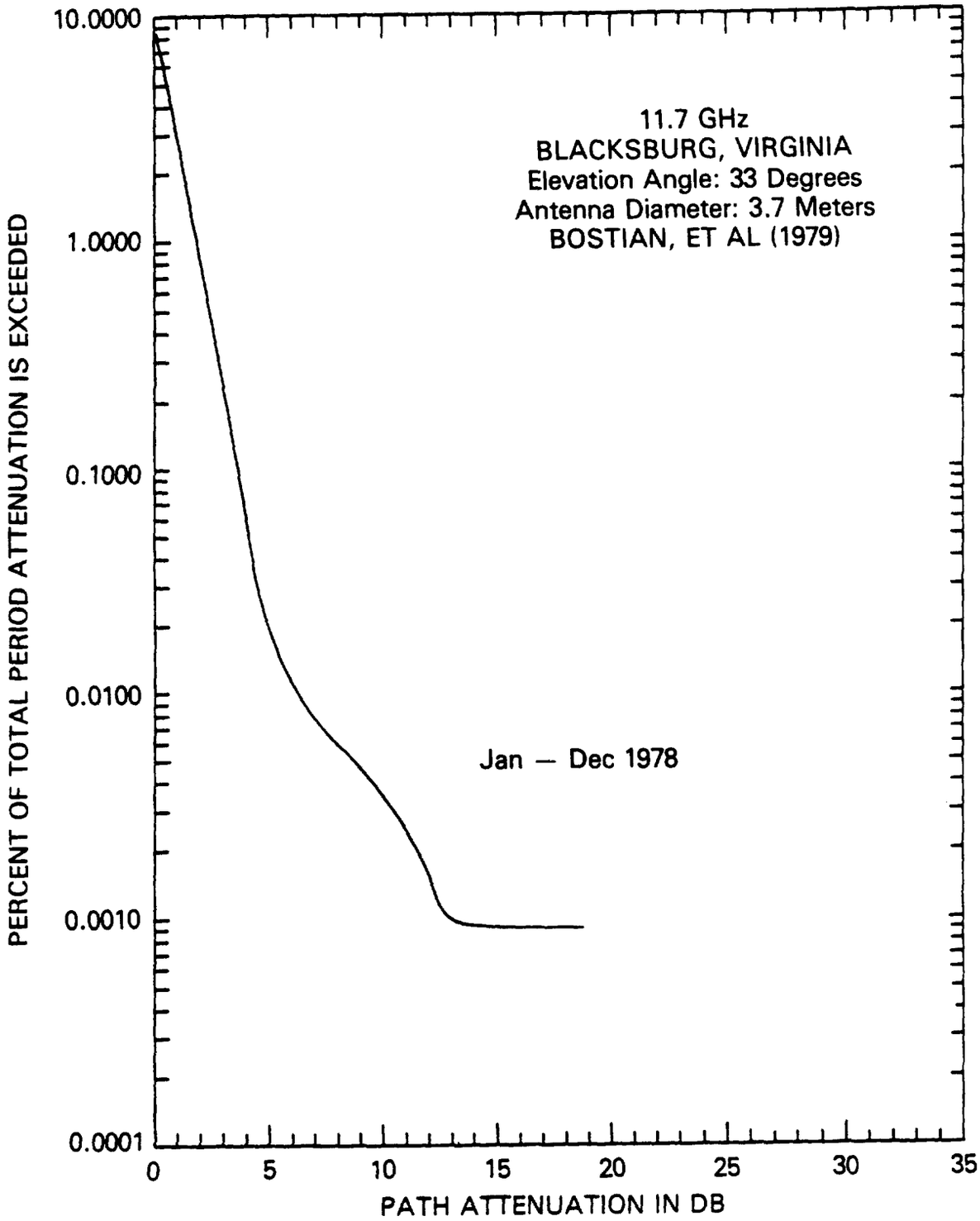

Figure 5.4-4. Annual 11.7 GHz Attenuation Distribution for Blacksburg, VA

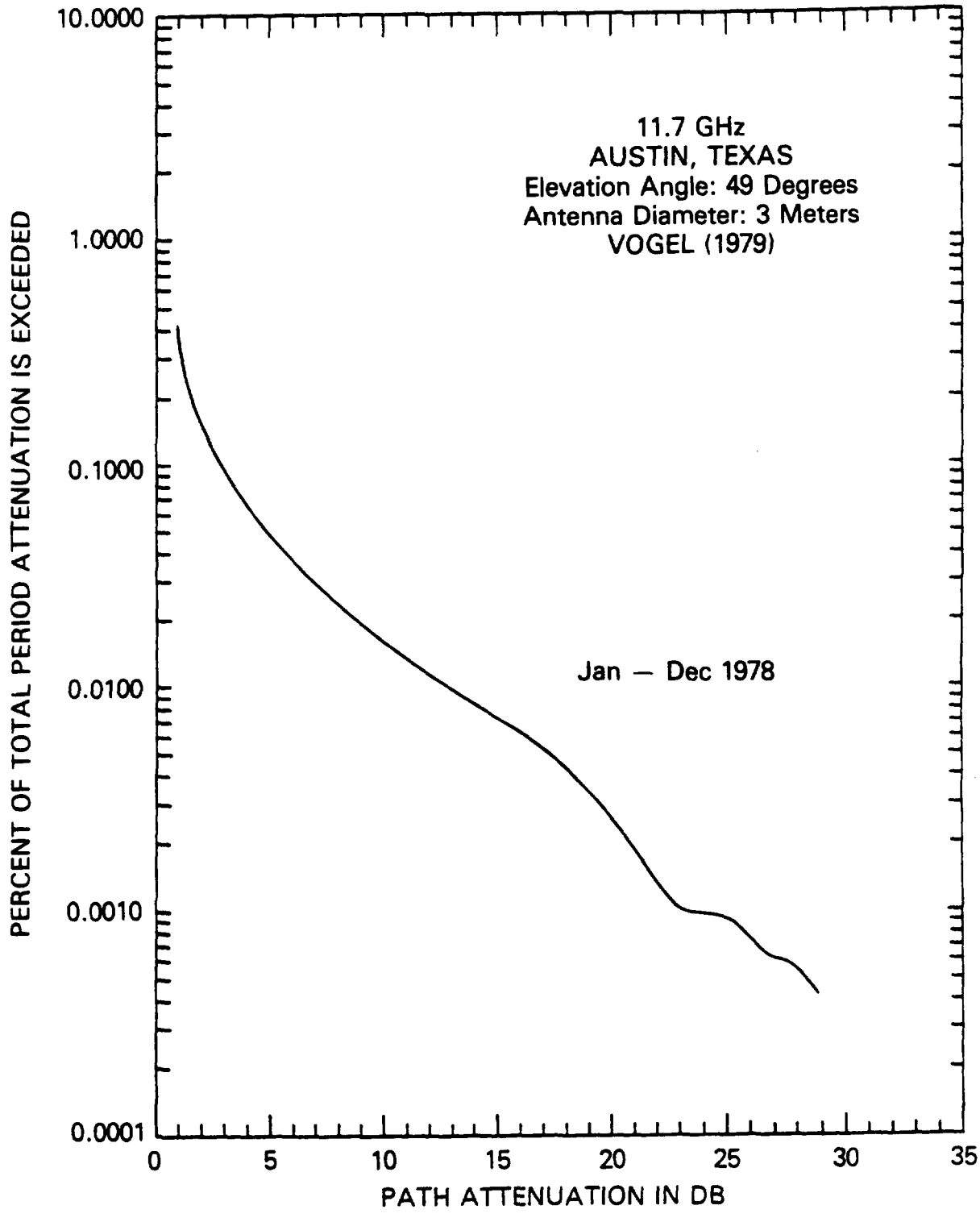

Figure 5.4-5. Annual 11.7 GHz Attenuation Distribution for Austin, TX

region of the elevation angle variations. Four of the sites have elevation angle differences of less than 9°; and, except for the 49° elevation angle at Austin, the sites differ by only a few degrees. Figure 5.4-6 presents annual 1978 distributions for each location converted to a 30 degree elevation angle. The distributions were converted to a 30° elevation angle by the relation

$$A_{30} = (\sin \theta / \sin 30^\circ)\ A_\theta \qquad (5.4\text{-}1)$$

where A_θ is the measured attenuation in dB at the elevation angle θ, and A_{30} is the attenuation at an elevation angle of 30°. The distributions for the two nearest locations, Greenbelt and Holmdel, show some similarity, while the distributions for Blacksburg and Waltham are significantly lcwer. Comparisons of this kind should be observed with some caution, however, since the distributions are based on only 12 months of continuous data, and local precipitation conditions will vary greatly from year to year (see above).

It is interesting to note, however, that all five locations are in similar temperate continental rain climate regions. Both the CCIR and global rain models place the five locations discussed here in the same climate zones. Thus, attenuation prediction models based on the two above referenced procedures would yield similar attenuation distributions for all five locations. Such a similarity is not evident for the measured annual distributions presented here for those five locations.

Figure 5.4-7 presents distributions at three locations where long-term measurements, extending from 29 to 36 months duration, were available. The long-term distributions are much smoother than the individual 12 month distributions, and the curves for Holmdel and Greenbelt are very similar, particularly in the region from .01 to .0025%, which is the area of great interest for system design margin criteria. The results point out the desirability for multi-year continuous measurements in the evaluation of rain attenuation effects on communications system performance.

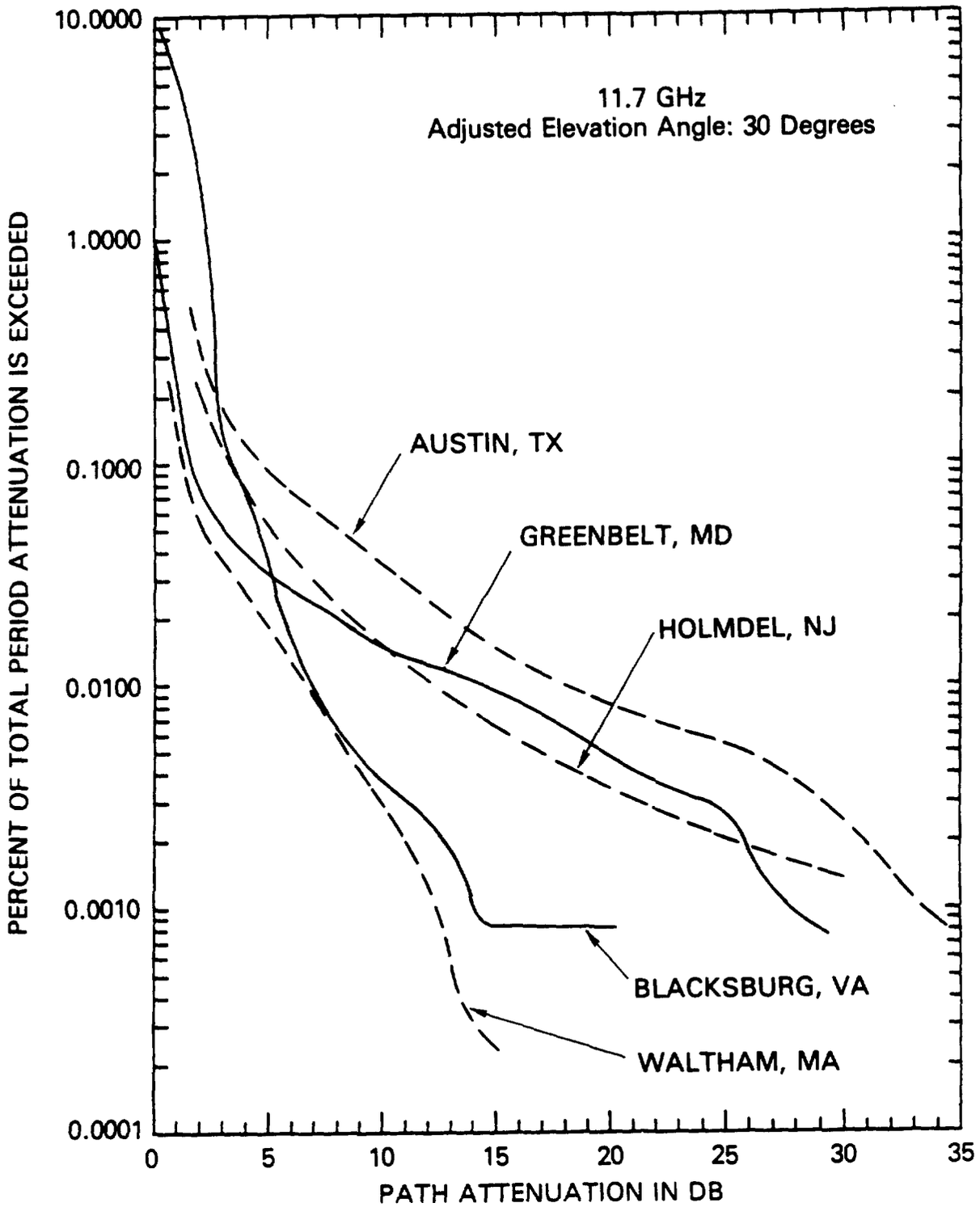

Figure 5.4-6. Comparison of 1978 Annual 11.7 GHz Attenuation Distribution of Measurements at Five Locations Adjusted to 30 Degrees Elevation Angle

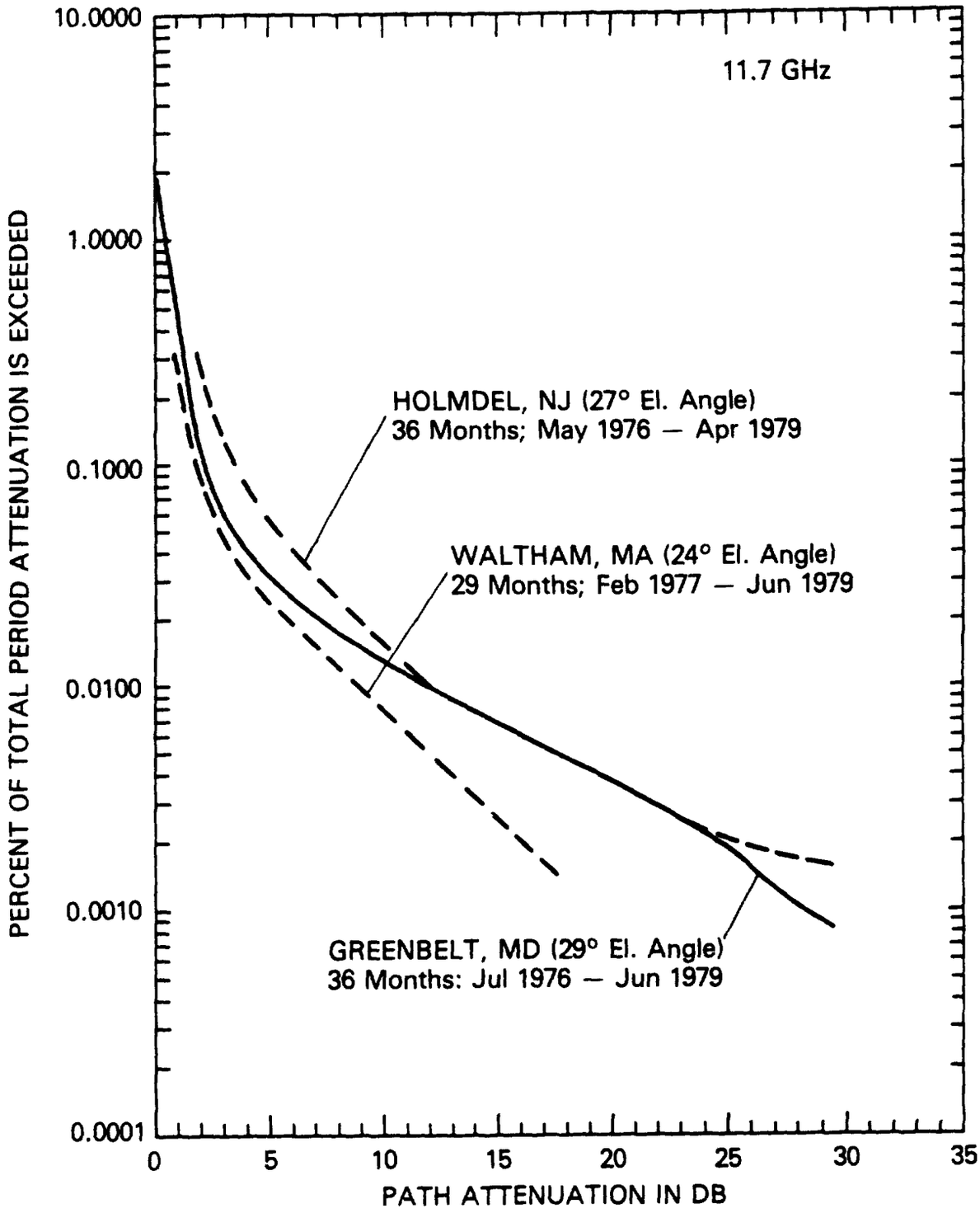

Figure 5-4.7. Long-Term 11.7 GHz Attenuation Distributions for Three Locations with Nearly Identical Elevation Angles

Representative European and Japanese attenuation data for frequencies near 11.7 GHz are shown in Figure 5.4-8 and -9. Figure 5.4-8 shows 11.6 GHz attenuation distribution curves for locations in Italy (Fucino, near Rome and Gera Lario, near Lake Como), France (Gometz-la-Ville, near Paris), and England (Slough, near London). Sources of these data are Macchiarella and Mauri (1980), Ramat (1980), and Davies (1981), respectively. Also shown is 11.5 GHz data for Japan (Kashima, on the coast east of Tokyo), from Hayashi (1979). Satellites used for the experiments represented here are SIRIO and ETS-II. Figure 5.4-9 presents data from an experiment in which separate antennas at the same station (near Darmstadt, Germany) simultaneously monitored 11.6 GHz beacon signals from the OTS and SIRIO spacecraft. The elevation angles of the two paths were within 4° of each other, but they differed by about 30° in azimuth. The large difference that is evident in the distributions has been attributed to orographic effects on local weather patterns: The SIRIO link passes over a hilly area for several kilometers while the OTS link lies over the Rhine river valley. These results (from Rucker - 1980) demonstrate the degree to which local climatic variations can affect rain attenuation statistics.

5.4.2 15-16 GHz Data

The 15 to 16 GHz experimental data base shown in Figure 5.4-10 is limited. The satellite beacon measurements were taken by NASA and COMSAT at North Carolina and Maryland. The earlier radiometer measurements by Bell Telephone Laboratories are included to supplement this satellite data. These radiometer measurements appear to agree with the satellite data up to 14 dB where the radiometer measurements stop because of sky temperature saturation. No other long-term 15 GHz data bases are known to exist in the U.S. or Canada. However, the Tracking and Data Relay Satellite System will eventually provide extensive data for 7 to 22 degree elevation angles from White Sands, NM.

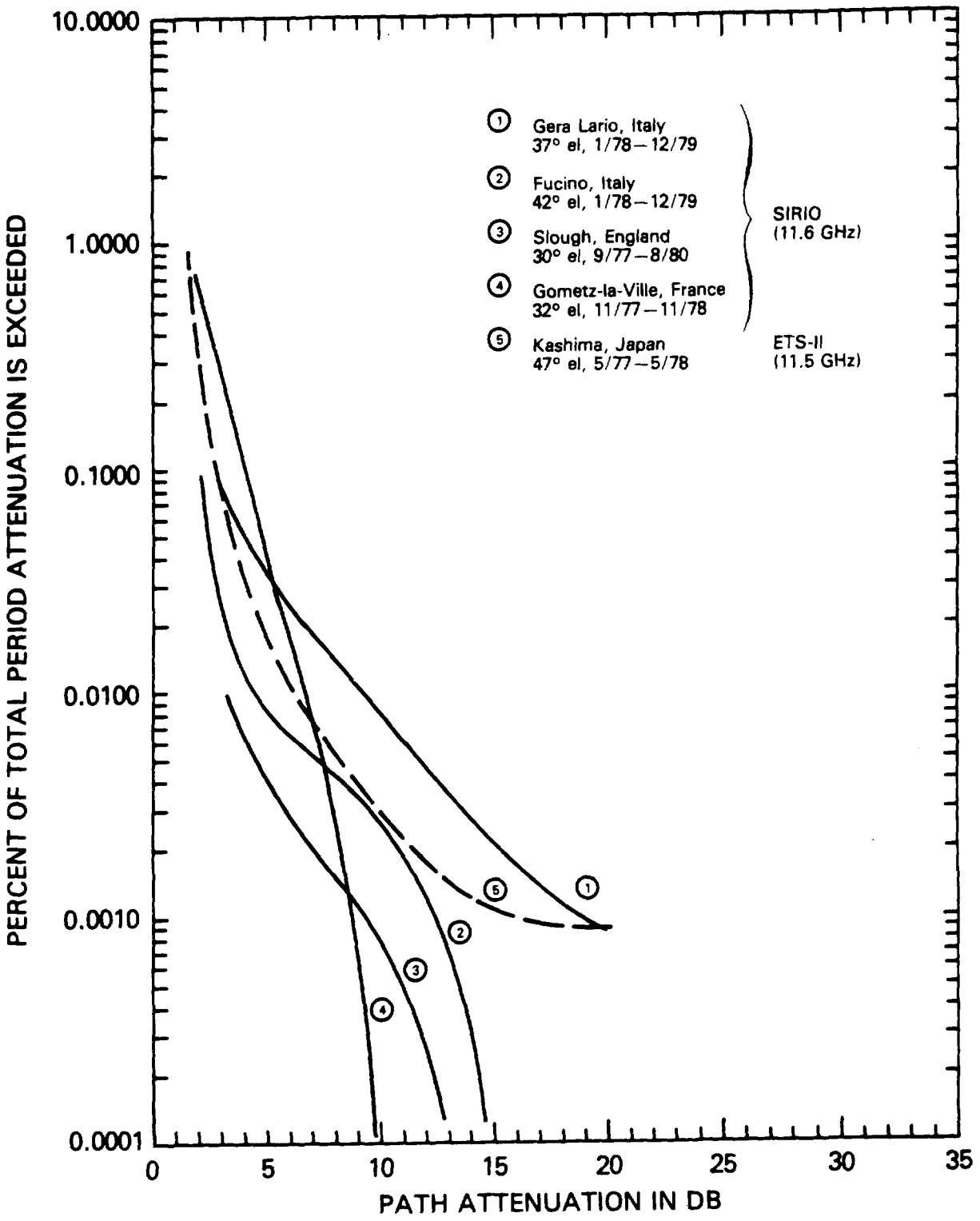

Figure 5.4-8. European and Japanese Attenuation Statistics for 11.5 and 11.6 GHz

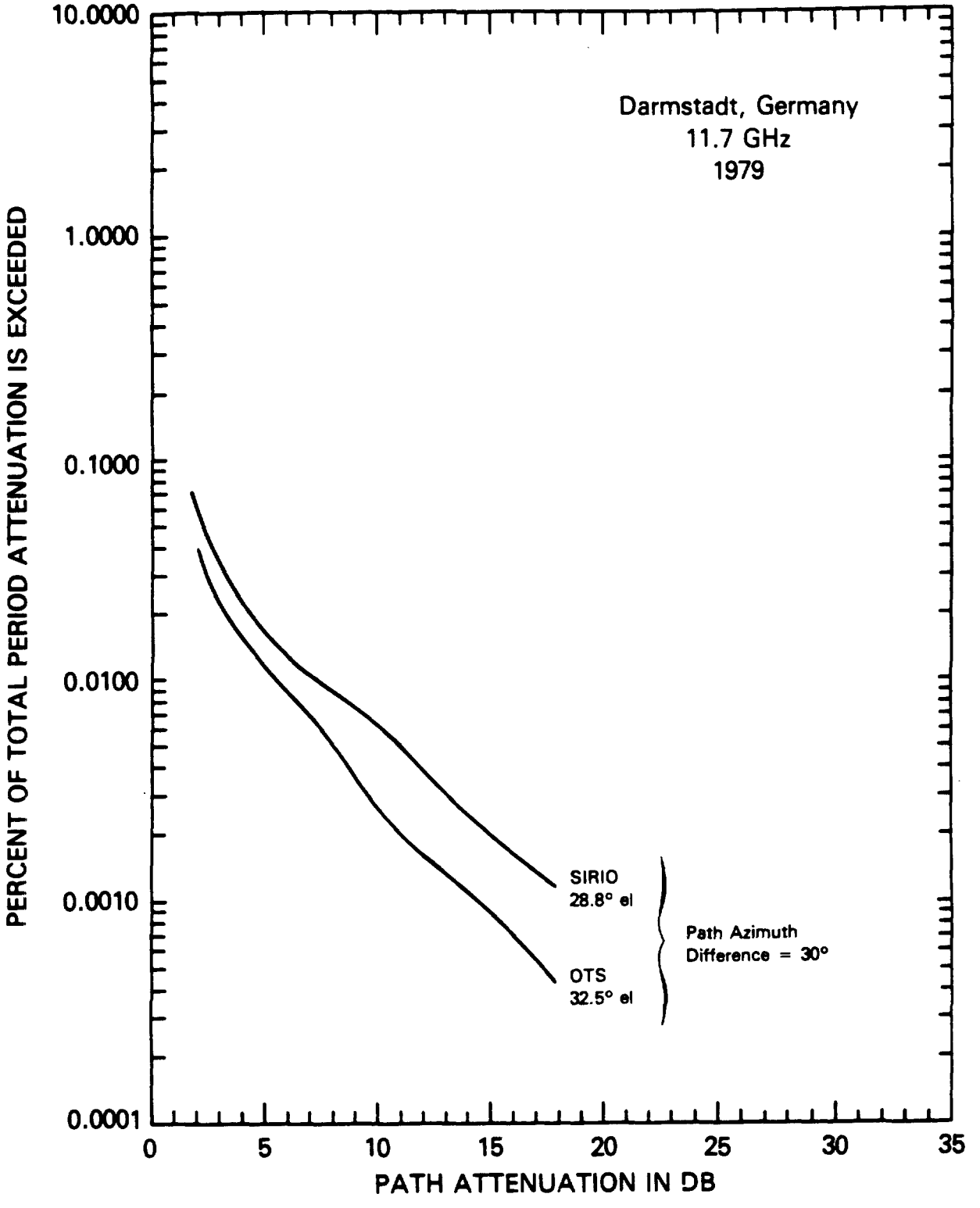

Figure 5.4-9. Simultaneous Attenuation Statistics for Two Paths from Same Earth Station

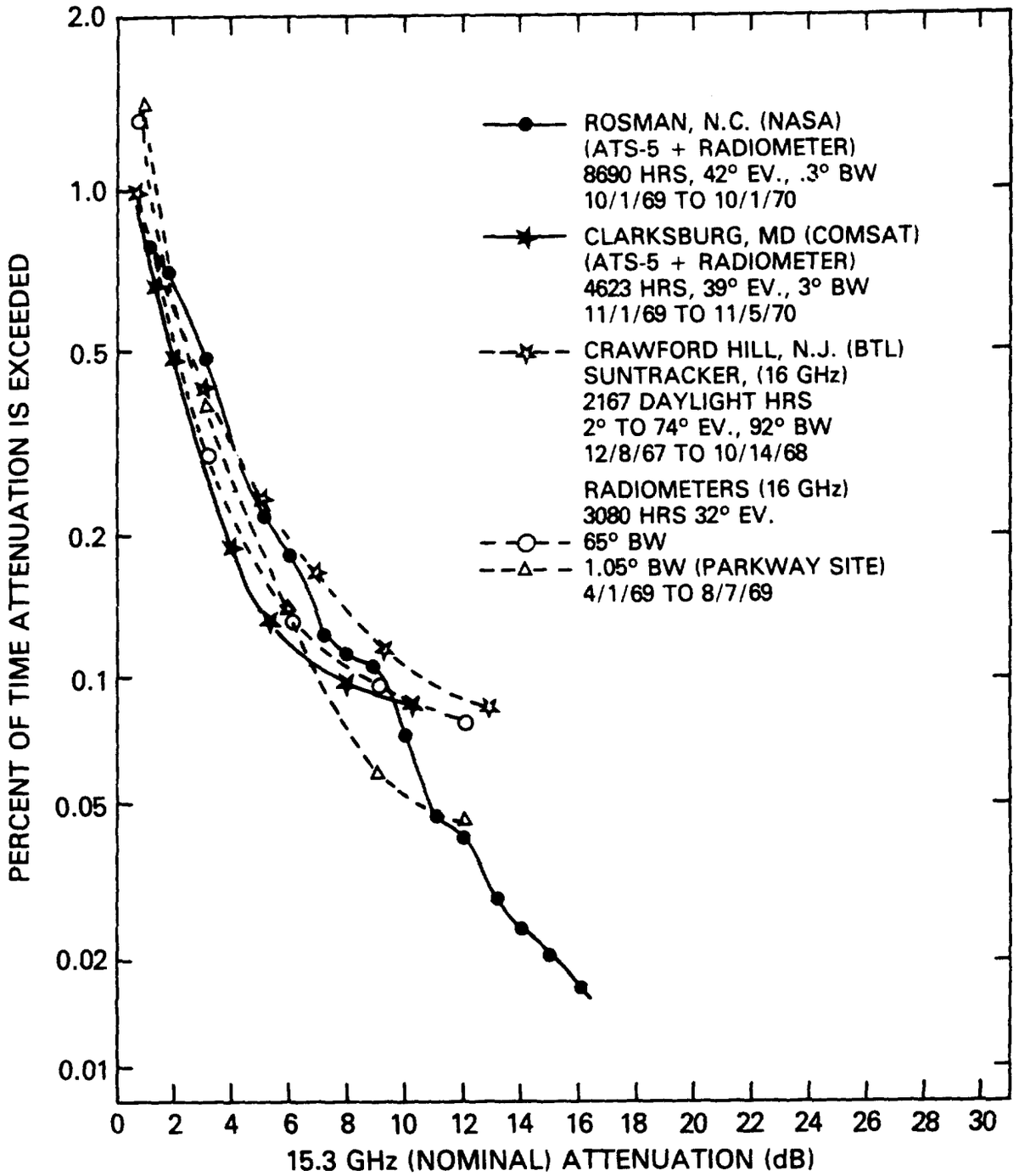

Figure 5.4-10. Summary of 15 GHz Measurements

5.4.3 19-20 GHz Data

Cumulative attenuation data in the 19 to 20 GHz range has been accumulated from both the ATS-6 and the COMSTAR beacons. In addition, the COMSTAR beacon has provided a source for direct measurement of depolarization.

The cumulative attenuation statistics at 19.04 and 20.0 GHz have been plotted in Figure 5.4-11. The Crawford Hill COMSTAR measurements (curve 2) included independent measurement of attenuation on nearly vertical (21 degrees from vertical) and nearly horizontal polarizations. Generally, horizontal and circularly polarized signals are attenuated more than vertically polarized signals. During 0.01% of the time, the COMSTAR measurements showed the horizontal attenuation to be about 2 dB greater than the vertical polarization (Cox, et al - 1979a). The polarization dependence arises because of the shape and general orientation of the raindrops. Also shown are the effects of hurricane Belle on the annual cumulative statistics. Clearly, this single event significantly shifts the curve for the moderate values of attenuation associated with heavy, but not intense, rain rates.

Figure 5.4-12 shows results from Japanese experiments using the 19.45 GHz beacon on the CS spacecraft.

5.4.4 28-35 GHz Data

The 28.56 GHz COMSTAR beacons and the 30 GHz ATS-6 beacon have provided excellent sources for attenuation measurements in the 30 GHz frequency region. The cumulative attenuation statistics for several locations in the U.S. are given in Figure 5.4-13. Japanese researchers have collected annual propagation data at 34.5 GHz with the beacon on the ETS-II satellite, as shown in Figure 5.4-12.

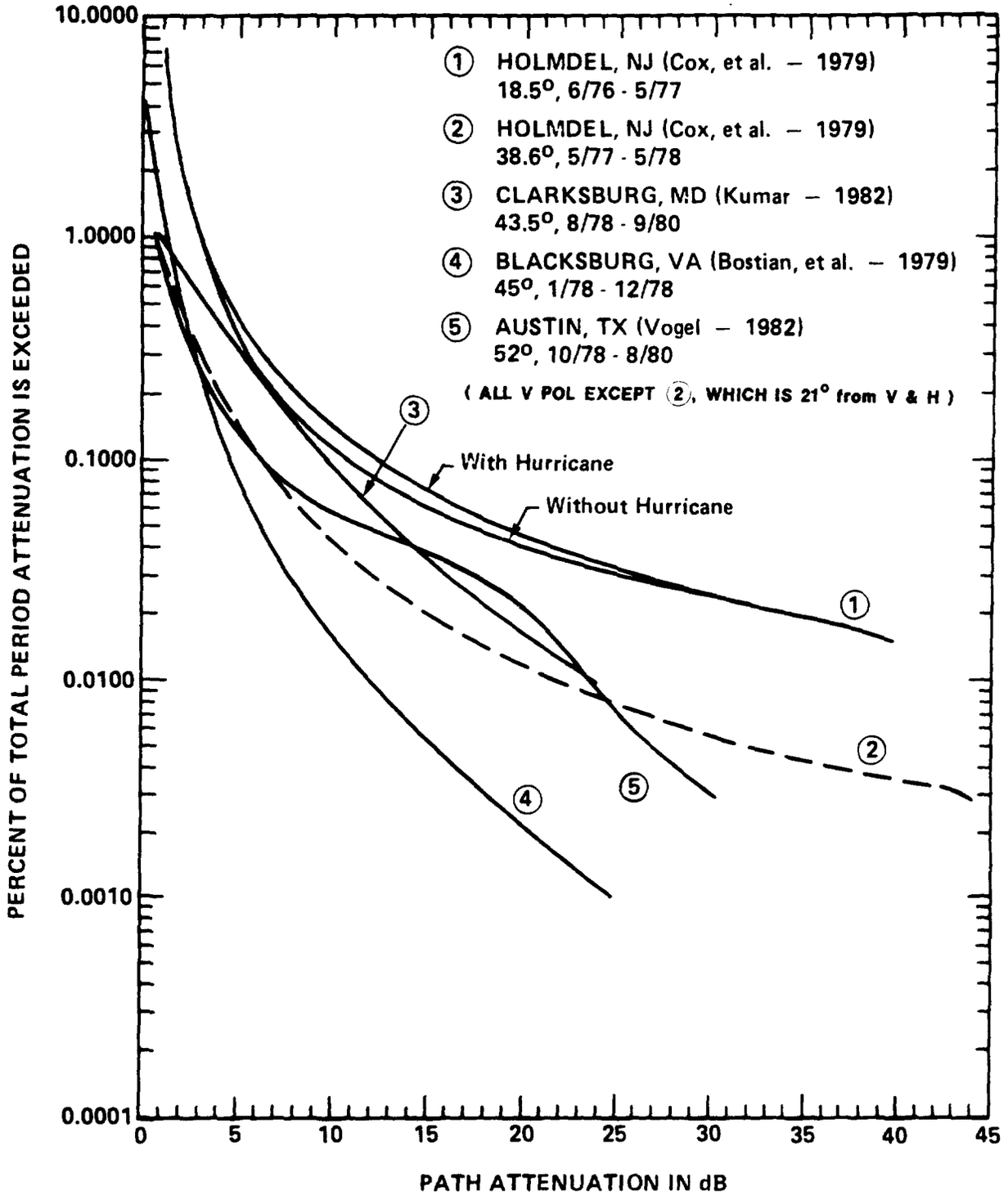

Figure 5.4-11. Summary of 19.04 and 20 GHz Measurements

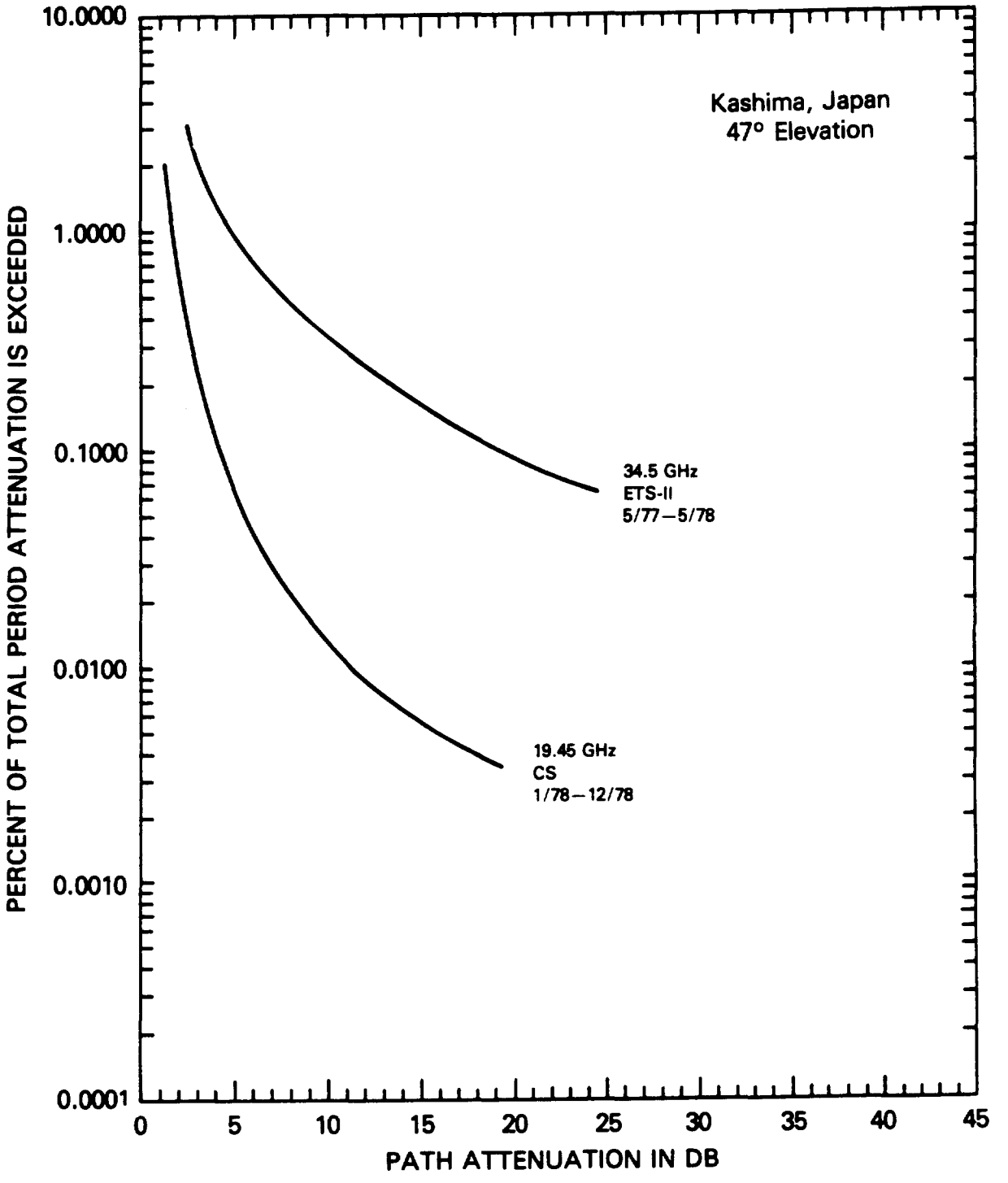

Figure 5.4-12. Results of Experiements with Japanese ETS-II and CS Beacons

5.4.5 Frequency Scaling of Attenuation Data

The relation between measured attenuations may be examined in several ways. The so-called statistical relation is obtained as a set of paired attenuations that are exceeded for equal amounts of time. These points may be obtained from the cumulative attenuation distributions. For the Crawford Hill measurements, for example, (Arnold, et al-1979) 19.5 dB attenuation at 19 GHz and 40.3 dB at 28 GHz were both exceeded for 65 min. This statistical relation is plotted in Figure 5.4-14 as a series of open circles for 19 and 28 GHz data for Crawford Hill.

The instantaneous attenuation relation may be determined from simultaneous data recordings of attenuation at the two frequencies. This instantaneous relation is also shown in Figure 5.4-14. The dashed curve indicates the median 19 GHz attenuation observed for values of 28 GHz attenuation on the abscissa. The bars in the figure indicate the span between the 10% and 90% points in the distribution of 19 GHz attenuations observed for the 28 GHz attenuation values. The quantization is 0.5 dB for the 10% and 90% points and for the median. Note that, while these results are statistical in nature as well, the quantity considered is the instantaneous attenuation for the two frequencies. It is evident from the figure that the statistical relation and the median instantaneous relation are essentially identical.

The dotted line on Figure 5.4-14 is the line for $A_2 = (f_2/f_1)^2 A_1 = 2.25A_1$ where A_1 is the attenuation in dB at frequency f_1=19.04 GHz and A_2 is the attenuation in dB at frequency f_2 = 28.56 GHz. The relationships between the measured attenuations depart from a frequency squared relation particularly at high attenuation. A straight line, $A_2 = 2.1A_1$ fits the data closely up to $A_1 \simeq 20$ dB but the data depart from this line at still higher attenuation. This less than frequency squared attenuation dependence is consistent with the frequency dependence of Chu's theoretical attenuation coefficients (1974) in this frequency range. The further decrease in frequency dependence at higher attenuations is consistent with

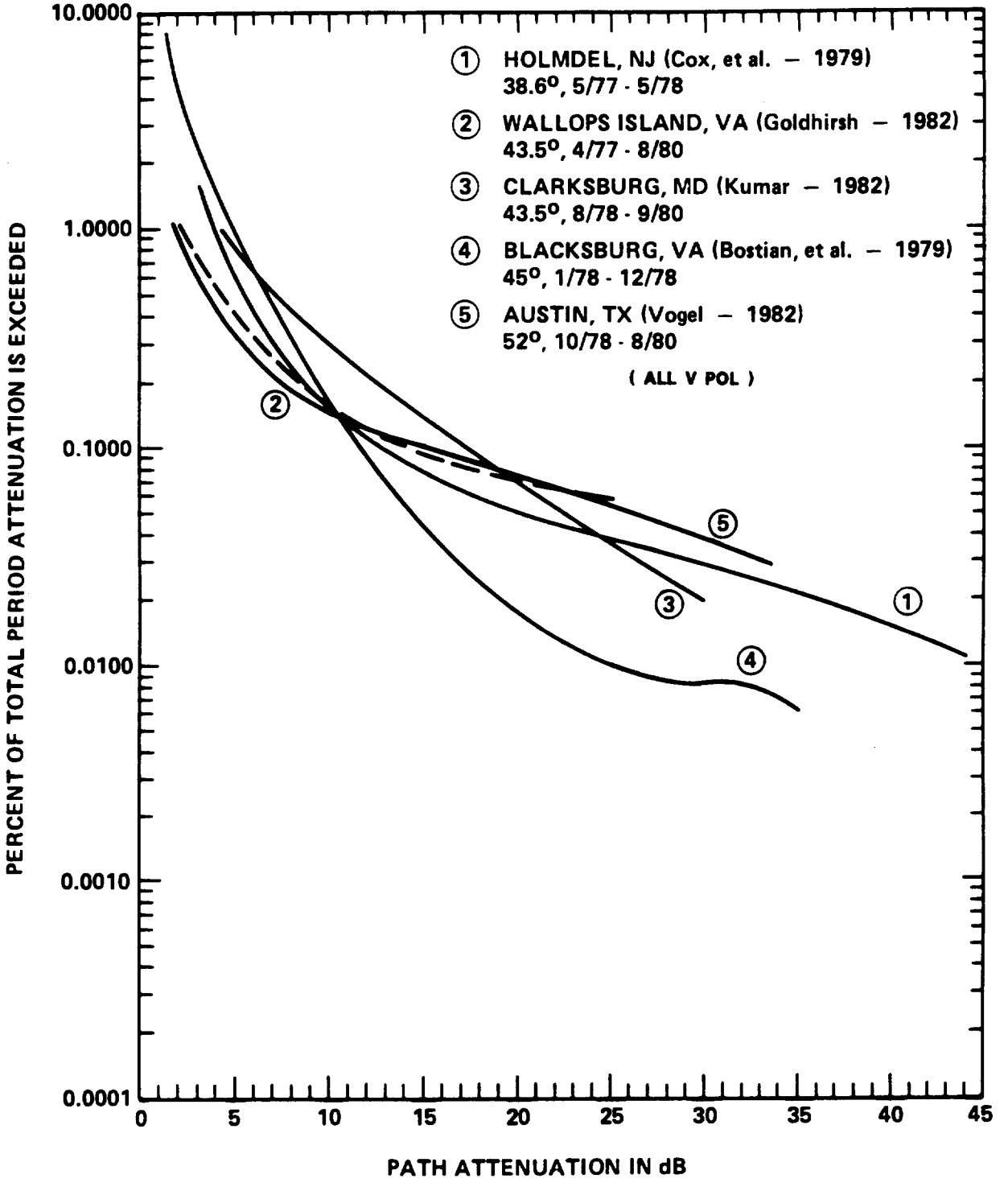

Figure 5.4-13. Summary of 28.56 and 30 GHz Measurements

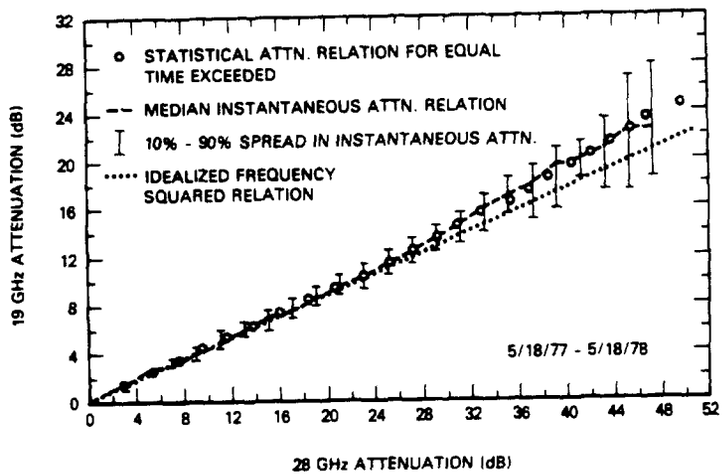

Figure 5.4-14. Relationships between 19 and 28 GHz Attenutation for Earth-Space Radio Propagation

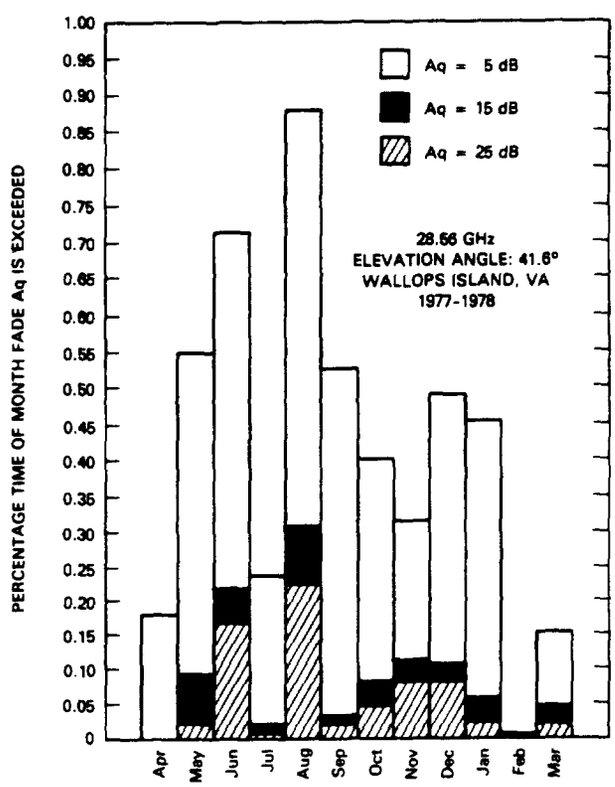

Figure 5.5-1. Histogram Denoting Percentage Times for Various Months the Fades of 5, 15, and 25 dB Were Exceeded

the same effect observed in the theoretical coefficients at higher rain rate since higher attenuation is associated with more intense rain.

In Figure 5.4-14, the increase in the spread between 10% and 90% points as attenuation increases is consistent with constant fractional fluctuation in the ratio of the attenuations at the two frequencies.

5.5 TEMPORAL DISTRIBUTION OF FADES

Systems may be able to accommodate fades during certain months or periods of the day more readily than during other periods. To help assess the magnitude of these effects along the eastern U.S. coast, Goldhirsh (1979, 1980) and others (Rogers and Hyde - 1979, Brussaard - 1977) have prepared histograms and cumulative distributions for various-months and times.

5.5.1 Monthly Distribution of Attenuation

Figure 5.5-1 shows the percentage of time for each month in the period April 1977 to March 1978 that fades of 5, 15, and 25 dB were exceeded. These measurements (Goldhirsh - 1979) were made at 28.56 GHz from the COMSTAR D2 satellite to Wallops Island, VA at an elevation angle of 41.6 degrees. The fades are more excessive during the summer months, except for July. This low value for July is not expected to be representative for that month and demonstrates how data from a single year can misrepresent the long-term average value.

Weather Bureau data may also be utilized to obtain this distribution by month, but this procedure may be inaccurate because the type of rain may vary significantly throughout the year. Some consideration to the amount of rainfall occurring in thunderstorms in a given month is needed to make these estimates more realistic. Ideally the rain rate distribution for each month would be required along with the attenuation models presented in Chapter 3. The variability of the statistics from year to year is demonstrated by a

comparison of the 1977-78 data with that obtained at Wallops Island in the September 1978-August 1979 period, using the COMSTAR D3 satellite (Goldhirsh - 1980). While the overall attenuation exceedance plots for the two periods agreed closely, several monthly exceedance values differed greatly between years. The percentage of July for which 15 dB was exceeded, for example, was about 0.3% in the 78-79 period compared with 0.02% in the 77-78 period. The 15 dB exceedance percentages differed by more than a factor of two between years for six of the twelve months.

5.5.2 Diurnal Distribution of Attenuation

One would expect severe fades to be most likely to occur during the late afternoon and early morning hours, when tropospheric heat exchange is the greatest and convective rains are most frequent. The 28 GHz COMSTAR data taken at Wallops Island, shown in Figures 5.5-2 and 5.5-3 (Goldhirsh - 1979), tends to confirm the expectation for the late afternoon. The figures show the attenuation statistics for the 1977-1978 period in terms of which 4-hour intervals of the day the attenuation was recorded. Figure 5.5-2 is a histogram giving time percentages for exceedance of 5, 15 and 25 dB attenuation values, and Figure 5.5-3 shows the complete cumulative distributions for each interval.

The time-of-day attenuation histogram of Figure 5.5-4 is from 11.7 GHz radiometer-based attenuation data at Etam, West Virginia (Rogers and Hyde - 1979). It shows two periods of the day dominated by deep, long fades, in early morning and late afternoon, as expected. The 11.4 GHz diurnal fade distribution given by Brussaard (1977) for a number of European locations exhibits a marked peak between 1500 and 1800 local time, but no peak in the morning. The 19.5 GHz 1979-80 data for Kashima, Japan shows a very different pattern (Fukuchi, et al - 1981), including a drop in deep fades at around 1700 local time. One-year data compiled at Palmetto, Georgia using the COMSTAR 19 GHz beacon, shows a broad minimum in the diurnal distribution of deep fades between about 0500 and 1000, and a broad peak between 1700 and 2300 (Lin, et al - 1980).

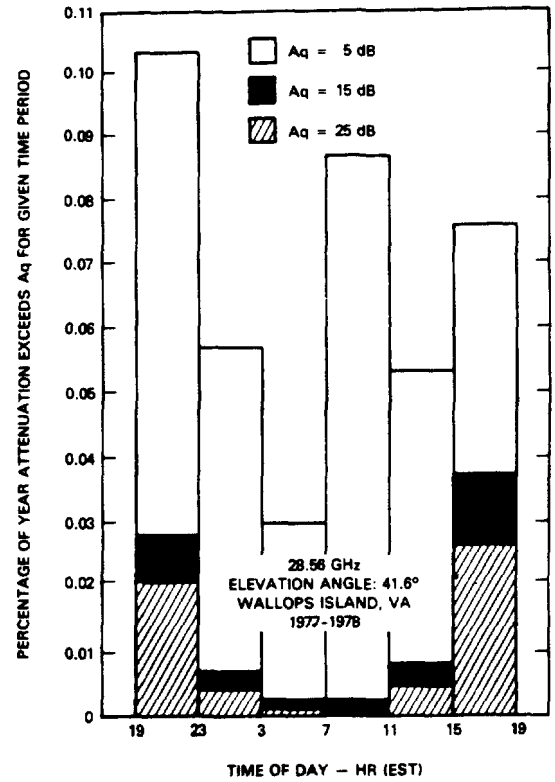

Figure 5.5-2. Diurnal Distribution of Fades Exceeding 5, 15, and 25 dB for Six Contiguous Four-Hour Time Slots of the Day

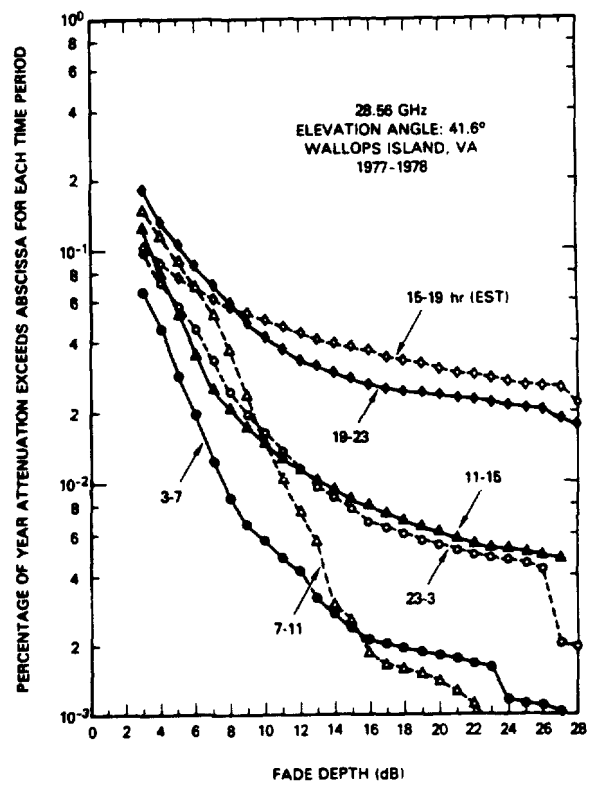

Figure 5.5-3 Cumulative Distributions for Six Contiguous Four-Hour Time Slots of Day

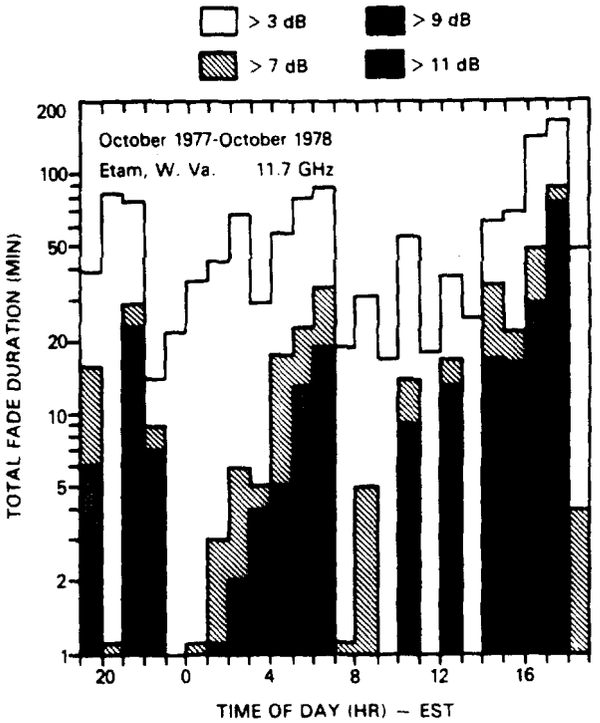

Figure 5.5-4. Diurnal Distribution of Fades Exceeding 3, 7, 9, 11 dB

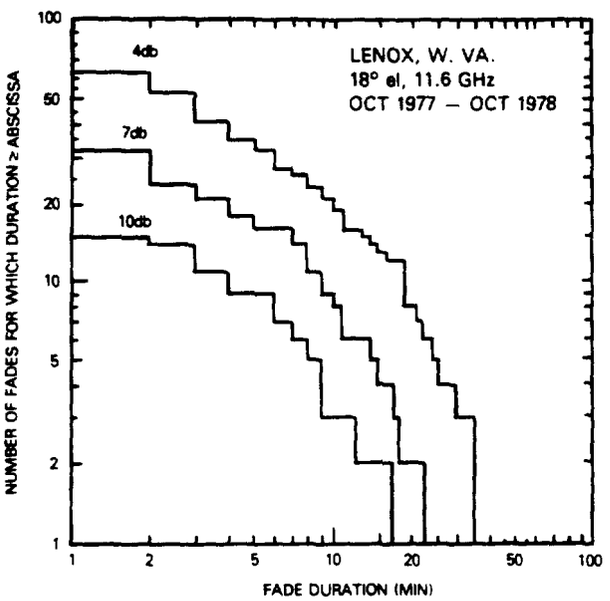

Figure 5.6-1. Histogram of Fade Duration From Radiometer Data

The diurnal distribution, like the monthly distribution, varies widely from year to year. Goldhirsh (1980) presents a comparison of diurnal distributions of the 1977-78 and the 1978-79 periods for 28 GHz attenuation at Wallops Island. In three of the six time intervals, the 15 dB exceedance percentage differed by more than a factor of two between the years.

5.6 FADE DURATION

Several experimenters have derived fade duration statistics for earth-space links. Rogers and Hyde (1979) present histograms of the number of fades exceeding specific depth and duration for 11.6 GHz at Etam and Lenox, West Virginia, based on a year's radiometer measurements. Figure 5.6-1 shows the Lenox histogram. Rogers (1981) gives similar data for Shimotsui, Japan, and in addition shows joint fade duration histograms for pairs of diversity sites in West Virginia and Japan.

Fade duration statistics have been compiled for 19 and 37 Gz at Slough, England, using a sun-tracking radiometer. Figure 5.6-2 shows histograms for fades exceeding 5 and 10 dB from the Slough data. Note that the method of presentation differs from that of Figure 5.6-1. The data in the earlier figure was the number of fades greater than or equal to the abscissa value, and the present figure gives the number with a length falling in one-minute intervals.

The use of a sun-tracking radiometer to estimate long-term path attenuation provides a greater range of measurement than a stationary sky-noise radiometer, but the data by necessity includes no night-time fading events. Also, due to the dependence of rain attenuation on elevation angle, a rainstorm occurring when the sun is low in the sky would produce deeper fades than an identical storm occurring closer to noon. Thus, long-term attenuation data from a sun-tracking radiometer is colored by the time of day that events producing fades tend to occur. One would expect this to limit its accuracy in describing statistics for a fixed elevation angle.

Fade duration statistics from direct attenuation measurements have been compiled by Japanese researchers for 11.5 and 34.5 GHz using the ETS-II satellite, shown in Figure 5.6-3, as well as limited 19.45 and 11.7 GHz statistics from the CS and BS experiments (Hayashi, et al - 1979).

Lin, et al (1980) present a summarization of fade duration data for 19 and 28.5 GHz on the COMSTAR (D2)-to-Palmetto, Georgia path. The durations of fades exceeding each of several attenuation thresholds between 5 and 25 dB at each frequency were normalized and presented on a single plot. The normalization consisted of dividing each fade duration value by the average duration for its frequency and threshold. The combined normalized data was shown to closely fit a log-normal distribution, which confirmed expectations.

5.7 EXPERIMENTAL DEPOLARIZATION DATA

The crosspolarization discrimination not exceeded for a given percentage of time, in decibels, is approximated by a relation (Nowland, et al-1977)

$$XPD = \tilde{a} - \tilde{b} \log_{10} (CPA) \qquad (5.7\text{-}1)$$

where CPA is the copolarized attenuation value in decibels exceeded for the same percentage of time. This suggests that the data be presented in a semilogarithmic format wherein each parameter is already a logarithm of another parameter. Therefore, in this Handbook we have replotted the results of others in order to present a uniform format of the data and to allow easy comparison with the CCIR approximation (see Eq. 4.3-27).

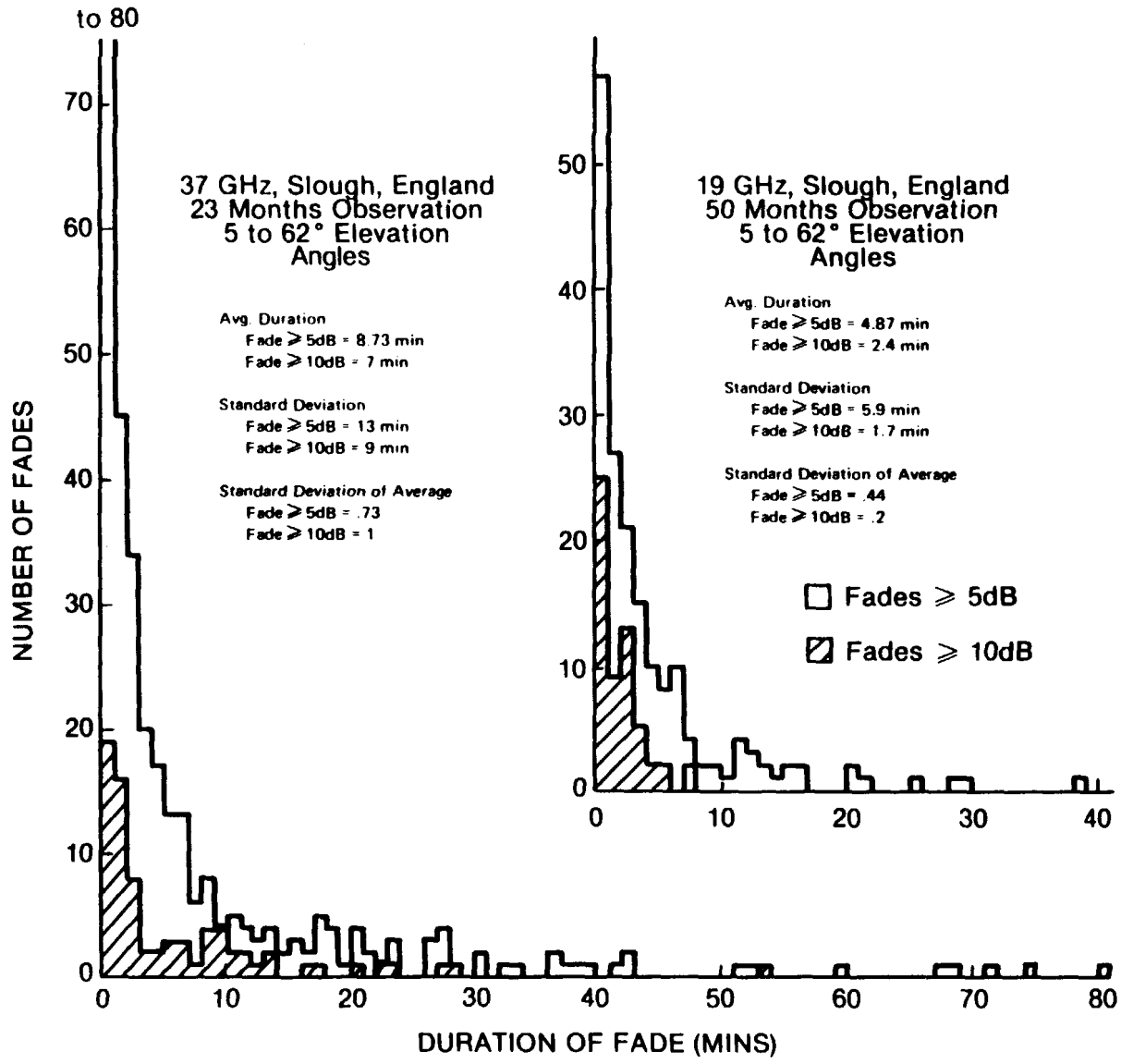

Figure 5.6-2. Histograms of Fades Greater Than 5 and 10 dB at 19 and 37 GHz

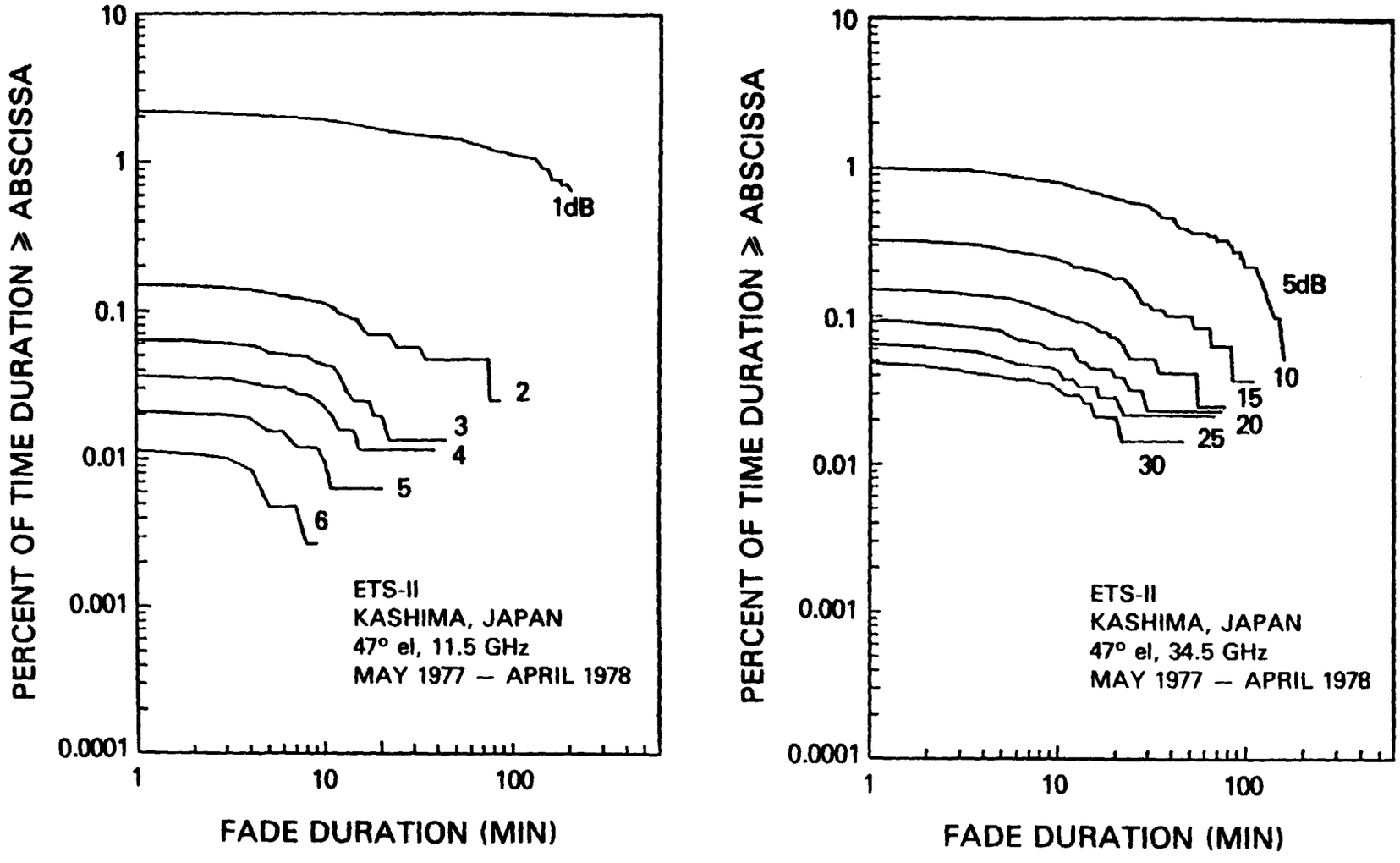

Figure 5.6-3. Fade Duration Statistics for Kashima, Japan, Obtained Using he ETS-II Satellite

5.7.1 19 GHz Data

Figures 5.7-1 and 5.7-2 present the 19 GHz cross-polarization data obtained by the Bell Laboratories experimenters at Crawford Hill, NJ (Arnold, et al - 1979). The near vertical polarization appears to have slightly more cross-polarization discrimination than the horizontal polarization. However, both polarizations show less discrimination than the CCIR estimate. Therefore, in this case, the CCIR approximation appears to be optimistic.

5.7.2 28 GHz Data

The COMSTAR signal at 28 GHz had a fixed polarization, thus allowing measurements at only one orientation with respect to the raindrop anisotropy. The data replotted from Bell measurements (Arnold, et al-1979) is shown in Figure 5.7-3. Again, the CCIR approximation is over-optimistic when compared to the measured data.

5.7.3 Joint Attenuation - Depolarization Data

Systems using orthogonal polarizations for frequency reuse suffer degradation due to crosstalk caused by depolarization in addition to the degradation due to rain attenuation. A full statistical description of the availability of such a system must consider the attenuation and depolarization jointly. Figure 5.7-4 (Arnold, et al - 1979) depicts such joint statistics for attenuation and depolarization on the 28 GHz COMSTAR-Crawford Hill Link. The figure gives the percentage of time that a given attenuation value was exceeded <u>or</u> a given XPD value was not exceeded. Note that the lower bound of all the curves is simply the attenuation exceedance curve, since it corresponds to low values of XPD, which happen a very low percentage of the time. Thus the location of this lower bound is established by attenuation alone. On the other hand, the curves become independent of attenuation for large values of attenuation, since the non-exceedance percentage for XPD far outweighs the exceedance percentage for attenuation.